Nanoscale

RSCPublishing

COMMUNICATION

Spatial modeling for refining and predicting surface potential mapping with enhanced resolution†

Cite this: *Nanoscale*, 2013, **5**, 921

Received 12th November 2012
Accepted 13th December 2012

DOI: 10.1039/c2nr33603k

www.rsc.org/nanoscale

Qiong Zhang,[a] Xinwei Deng,[b] Peter Z. G. Qian*[a] and Xudong Wang*[c]

Quantitatively mapping surface properties with nanometer or even subnanometer resolutions is critical for advanced scanning probe microscopy (SPM) characterization. However, the characterization performance often suffers from noises and artifacts due to instrumentation or environmental limitations. In this paper, we proposed a novel statistical approach with bivariate spatial modeling to efficiently refine and predict surface property mapping. Scanning Kelvin probe microscopy (SKPM) was selected as a representative example to test our proposed method on lateral nanowire assemblies. We revealed that the proposed method can effectively retrieve the artifact-free surface potential distribution by automatically identifying topological artifacts from surface potential maps. Furthermore, the statistical model built upon low spatial resolution was successfully used to predict the potential values from higher-resolution topography data. Compared to conventional regression model, our model is able to predict the surface potential distribution from less raw data but yields much higher accuracy. Through this means, the spatial resolution of SKPM surface potential maps can be significantly improved. This statistics-enabled predictive method opens a new route toward high-precision and high-resolution SPM characterizations without the enhancement of instrumentation capabilities.

Introduction

Scanning probe microscopy (SPM) is a powerful and versatile technique for nanoscale surface property characterization. By designing the interaction between an ultrafine scanning tip and the surface, SPM can be used to probe and map a large variety of properties on material surfaces, including topography, electrical potential, electrical and thermal conductivity, mechanical strength, piezoelectric response, magnetism, electrochemical activity, to name but a few.[1–7] Because of the highly localized response during probing, SPM-based techniques are particularly useful for identifying property variations and distribution related to surface topography, structure, or composition. This unique capability has found great promise in current nanotechnology and energy technologies by offering nanomaterial scale quantification of the photovoltaic effect, the thermoelectric effect, ferroelectric domain orientation, the piezoelectric potential output, catalytic performance, and ionic transport.[8–10] To facilitate these cutting-edge applications, the probing precision and spatial resolution are of critical importance.

Theoretically, the spatial resolution of SPM is determined by the size of the probe tip, which is typically in a range of a few nanometers. However, the high sensitivity of the tip–surface interaction also makes the recorded signal extremely vulnerable to disturbance, which is one of the most critical issues that restrict the precision and reliability of SPM characterization.[11–13] Topography and force field are the two most common disturbances to SPM characterization: the former often results in topographical artifacts; the latter is the main cause for lower spatial resolution of property mapping. Our recent research showed that statically approaching the surface from the third dimension instead of lateral scanning can effectively minimize the topographic artifact by sacrificing probing time and spatial resolution.[14] Nevertheless, topographical artifacts due to high surface roughness still seriously affect the accuracy of raster scanning over a surface for constructing a two-dimensional (2D) property map with nanometer-scale spatial resolution.[15,16] Even with flat surfaces, surface property mapping often exhibits lower spatial resolution compared to topographical mapping.[17] This is because topography is acquired based on the van der Waals force which is highly localized beneath the probe tip ($\sim$1 nm). But for property mapping, the necessary force fields, such as the electric field, temperature, magnetic field, would influence the probe feedback in a range of 10 nm or even 100 nm.[18] Environmental disturbance could also easily affect such force fields, and further raises uncertainty and lowers the resolution.

[a]Department of Statistics, University of Wisconsin-Madison, USA. E-mail: peterq@stat.wisc.edu

[b]Department of Statistics, Virginia Polytechnic Institute and State University, USA

[c]Department of Material Science & Engineering, University of Wisconsin-Madison, USA. E-mail: xudong@engr.wisc.edu

† Electronic supplementary information (ESI) available. See DOI: 10.1039/c2nr33603k

These limitations for advanced nanoscale SPM characterizations are mostly intrinsic to their operation principles. To overcome this obstacle and realize nanometer-resolution artifact-free SPM property mapping, it may require new mechanisms and principles that can be extremely challenging. On the other hand, the statistics-guided approach is a new strategy for precise uncertainty quantification in materials science. Recently, statistical methods have been successfully applied to tackle challenging problems in nanotechnology.[19–28] For example, Dasgupta *et al.*[19] proposed a novel multinomial generalized linear model for analyzing the synthesis experimental data to achieve robust and optimal synthesis conditions. Also, Deng *et al.*[20] developed sequential profile adjustment by regression (SPAR) to account for and filter out various experimental errors and artifacts, thus giving more precise estimation of the elastic modulus of ZnO nanobelts. Different from the regression models in the previous literature, the major challenge of this work is to seek an effective spatial model for surface quantification at the nanoscale level. To this end, we propose a new statistics-based approach to model the two-dimensional potential surface. The proposed method can effectively identify topological artifacts and retrieve the actual surface potential distribution of lateral nanowire (NW) assemblies. Moreover, we can improve the spatial resolution of potential mapping by property prediction from higher-resolution topography data. This strategy opens a new route toward high-resolution SPM characterizations without the enhancement of current experimental capabilities.

Experimental setting

Scanning Kelvin probe microscopy (SKPM) was selected as an example of the SPM technique. In our experiments, SKPM was used to map the surface potential distribution on random lateral NW assemblies. SKPM is able to provide quantitative values of surface potential by determining the potential difference between the conductive probe tip and the sample surface. The basic operation setup of SKPM is schematically illustrated in Fig. 1a, where an AC signal and a DC voltage offset (VDC) are applied toward a conductive atomic force microscopy (AFM) tip. The silicon substrate is grounded and VDC is adjusted to minimize the cantilevers oscillation amplitude induced by the potential difference between the tip and the sample surface. By recording the VDC value required to maintain this condition at all points during the raster scan of the surface, the image of surface potential is obtained. Meanwhile, the topography image is acquired during the non-contact raster scanning mode.

Fig. 1b and c show the topography and surface potential data measured on three ZnO NWs placed on a silicon substrate, respectively. The data are measured on a 256 × 256 grid with 256 points taken from the u-axis (0–4.668 μm) and 256 points taken from the v-axis (0–1.556 μm). Therefore, a total number of 65 536 = 256 × 256 points are obtained from the sample surface to construct the topography and potential maps. From Fig. 1b, the morphology and location of the three NWs (with topography values varying from −100 to 150 nm) can be clearly identified from the substrate (with topography values varying from −250 to −100 nm). However, the corresponding potential map is fairly rough (Fig. 1c). The surface potential distribution is noisy and not well registered to the topography due to the resolution issue of SKPM.[11] A sharp change of potential can be clearly observed along the NW edges, indicating a typical topography artifact that resulted from additional forces sensed by the AFM tip when it reaches or leaves the abrupt edge of the NW (see Fig. 1a for example).[29] However, the ideal surface potential mapping should show two different constant potential values for the NWs and the substrate respectively, because of the different work functions of ZnO and Si. Therefore, it is crucial to recover the true potential distribution from the noisy and defective raw data, which is a substantial objective for statistics-enabled predictable SPM nanoscale surface analysis.

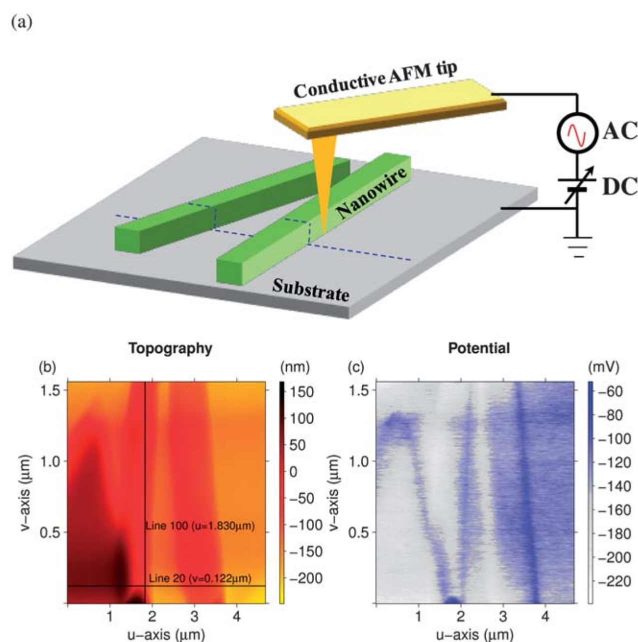

Fig. 1 (a) Schematic setup of SKPM measurement. (b) Topography image (nm) measured under non-contact raster scanning mode. (c) Potential image (mV) measured by SKPM during the raster scan of the sample surface.

Spatial model

Primarily, we consider how to model the relationship between the topography surface shown in Fig. 1b and the potential surface shown in Fig. 1c. We first define several statistical notation. Let $z(u,v)$ (mV) and $x(u,v)$ (nm) denote the potential value and the topography value on the location (u,v) respectively, where (u,v) is the location label on the micro-meter scale. Data are observed on the 256 × 256 grids (u_i,v_j), $i,j = 1, \ldots, 256$, where u_i is the location on the u-axis and v_j is the location on the v-axis, respectively. Since the ideal potential distribution is driven by the locations of the three NWs, it is legitimate to consider that

$$z(u,v) = f_z(u,v) + \delta(u,v), \quad (1)$$

 This journal is © The Royal Society of Chemistry 2013

where $f_z(u,v)$ is a deterministic function with respect to the location (u,v) of the sample surface. Here, $f_z(u,v)$ reflects the ideal performance of the potential distribution. The second term $\delta(u,v)$ is the random error whose distribution mainly stemmed from the location (u,v). It accounts for the noise caused by experimental disturbance, *e.g.*, van der Waals force, electric fields, and so on. Similarly, the topography value can be expressed by:

$$x(u,v) = f_x(u,v) + e(u,v), \tag{2}$$

where $f_x(u,v)$ is also a deterministic function and $e(u,v)$ is a random variable related to the subtle variation of the topography surface shown in Fig. 1b. As mentioned previously, both topography and potential surfaces are expected to reflect a sharp contrast between the NWs and the substrate. Hence $f_z(u,v)$ in eqn (1) should be more or less dependent on $f_x(u,v)$ in eqn (2). Moreover, the variance of $e(u,v)$ is expected to be much smaller than that of $\delta(u,v)$ because the topography surface is measured more accurately under non-contact scan mode. As a result, when modeling the relationships between $z(u,v)$ and $x(u,v)$, we consider retrieving the function $f_z(u,v)$ from $x(u,v)$, and therefore the proposed model will omit the random error $e(u,v)$ of the topography surface.

Before unfolding the proposed model, here are two cross-sectional examples to illustrate the relationships of the two surfaces. The first one is the horizontal scanning at line 20 ($v = 0.122$ μm) from Fig. 1b. As shown in Fig. 2a, the topography curve rapidly declines at $u = 1.700$ μm and $u = 3.700$ μm, which represents the boundary points between the NW and the substrate. On the topography curve, we observe two local peaks around the corresponding locations ($u = 1.700$ μm and $u = 3.700$ μm). Moreover, the sharp drops in the topography line often take place ahead of the local peaks on the potential curve. Such findings suggest that the derivatives of the topography are useful in modeling the potential surface. The second example is the line extracted along the direction vertical to scanning at $u = 1.830$ μm shown in Fig. 1b. As shown in Fig. 2b, the curve from topography resembles the pattern of the potential curve. Both examples indicate that the potential value on a single location is closely correlated to the observations of its neighborhood locations in both directions. Consequently, such spatial dependency would be essential in order to properly model the potential surface $z(u,v)$ in eqn (1).

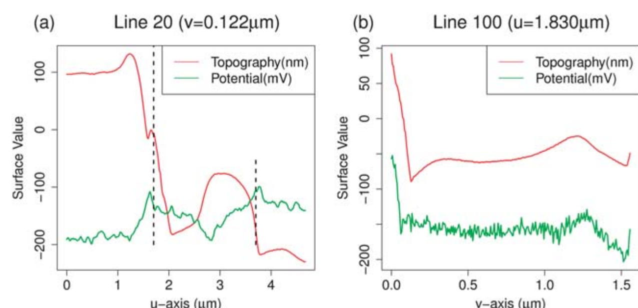

Fig. 2 Two lines of the surface data. (a) Line 20 in the scanning direction ($v = 0.122$ μm). (b) Line 100 vertical to the scanning direction ($u = 1.830$ μm).

For appropriately quantifying the spatial dependence of the potential surface and its relationship with the topography surface, we propose a new spatial model by modifying the kriging approach.[30] The kriging method is a popular technique in geostatistics, and is also widely applied to approximate computer models.[31,32] Our proposed model can be written as

$$z(u,v) = \mu + g(u,v)^{\top}\beta + \varepsilon(u,v), \tag{3}$$

where $\mu + g(u,v)^{\top}\beta$ is the mean of the potential surface, $\mu \in R$ and $\beta \in R^d$ are unknown parameters, $g(u,v) = \{g_1(u,v), \ldots, g_d(u,v)\}^{\top}$ is a d-dimension function, and $\varepsilon(u,v)$ is the random term with spatial dependence through the experimental region. We adopt the commonly used product correlation function for $\varepsilon(u,v)$ in spatial analysis:[33]

$$\begin{aligned} E\{\varepsilon(u,v)\} &= 0 \text{ and } \operatorname{cov}\{\varepsilon(u,v),\varepsilon(u',v')\} \\ &= \sigma^2\gamma(|u-u'|,\theta_u)\gamma(|v-v'|,\theta_v), \end{aligned} \tag{4}$$

where $\gamma(r,\theta)$ is a function decreasing with r, and θ_u, θ_v and σ are the parameters in the covariance structure. In this work, we specify $\gamma(r,\theta)$ to be $\exp(-\theta r)$, which refers to the power exponential correlation function.[34] Other specifications of $\gamma(r,\theta)$ can be found in Stein (1999).[35] The modeling details are derived in the ESI S1.†

Note that, without the spatial dependence, the covariance structure in eqn (4) becomes

$$\operatorname{cov}\{\varepsilon(u,v),\varepsilon(u',v')\} = I(u=u')I(v=v'), \tag{5}$$

where $I(\cdot)$ is an indicator function. Under eqn (5), the proposed approach is simplified as the traditional regression model which uses least squares for parameter estimation.

In the proposed model (3), the term $g(u,v)^{\top}\beta$ links f_z in eqn (1) and f_x in eqn (2). Scientifically, $g(u,v)$ would gain the capability of predicting the expected potential value. For the choice of $g(u,v)$, we consider a vector with components of $x(u,v)$, $\partial x(u,v)/\partial u$, and $\partial x(u,v)/\partial v$ based on the elaboration shown in Fig. 2. Here, we use numerical methods to approximate the derivatives. Details are provided in the ESI S1.†

Case study: refining the potential map

Taking into account of computing the derivatives of topography, the sample surface has shrunken to 252 × 252 grids due to getting rid of the edge points where the derivatives are inestimable. By fitting the model in eqn (3) using the 252 × 252 grid points, the expected potential surface is estimated by

$$\begin{aligned} \hat{f}_z(u,v) = &-156.034 - 0.014 \times x(u,v) + 1.264 \times 10^{-4} \times \partial x(u,v)/\partial u \\ &+ 2.868 \times 10^{-5} \times \partial x(u,v)/\partial v. \end{aligned} \tag{6}$$

Fig. 3a presents the recovered potential surface by using the estimation of $f_z(u,v)$ in eqn (6). The sharp potential ridge along the NW's edge in Fig. 1c is completely removed. The NW and the substrate surfaces are also clearly distinguished by their uniform potential values: the potential value of substrate is around −153 mV, whereas the potential values of the NWs are

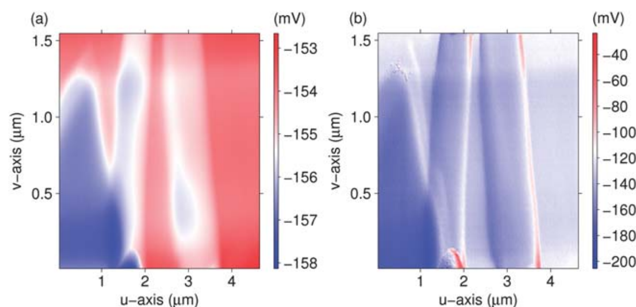

Fig. 3 Expected potential surfaces. (a) Recovered by the proposed method. (b) Recovered by the traditional regression model.

mainly from −158 mV to −155 mV. Given both the NW and substrate surfaces are grounded, they are expected to exhibit zero surface potentials that are very close to each other. The recovered potential values therefore are able to reflect the actual potential distribution on such a complex surface morphology. The ∼155 mV offset is attributed to the finite tip–sample distance during SKPM characterization. In contrast, Fig. 3b shows the retrieved surface from the traditional regression method with covariance structure in eqn (5). Comparing Fig. 3a and b, the recovered surface from traditional regression is clearly not as smooth as that estimated by the proposed method. For example, high potential value still appears along the NW boundaries (red and white regions in Fig. 3b). The recovered surface potential also exhibits much larger variations from −200 mV to −40 mV. This comparison clearly evidences that the proposed model outperforms the traditional regression in recovering the expected potential surface.

Case study: predicting the potential surface

As we discussed before, the potential mapping always exhibits lower spatial resolution compared to surface topography map. Therefore, another important application of the proposed

Table 1 Examples for prediction of the potential surface

Example	Data for model building	Percentage (%)
1	13 × 13	0.27
2	26 × 26	1.06
3	63 × 63	6.25
4	126 × 126	25.00

model (3) is to predict the surface potential distribution with high resolution by utilizing information from the topography data.

To evaluate the prediction performance of the proposed method, we consider estimating the predictive model using the experimentally measured lower-resolution potential data, and then predict the potential surface using the higher resolution topography data. The prediction accuracy of the proposed method is examined by comparing the predicted potential values with the true values. In statistical terminology, the data used in model estimation are called the training set and the data used for evaluating the predictive performance are called the test set. For illustration, we split the original dataset into two parts: one for the training set and the other for the test set. Table 1 summarizes the resolutions of the training data in the four examples. In examples 1–4, the training sets contain 169 (=13 × 13), 679 (=26 × 26), 3969 (=63 × 63) and 15 876 (=126 × 126) locations respectively. They are used to generate the potential maps with different spatial resolutions. Fig. 4a–d present the images of the potential maps of examples 1–4 in the order of incremental resolution. The distribution of the selected points is described in Fig. S1 of the ESI.†

For evaluating the prediction results, we report the prediction error of the potential surfaces through heat maps in Fig. 4e–h. As indicated in Fig. 4e–h, the predictive power of the proposed method is improved by gathering more training points in model fitting. For the lowest resolution surface (Fig. 4a), the predictive error in Fig. 4e roughly ranged from

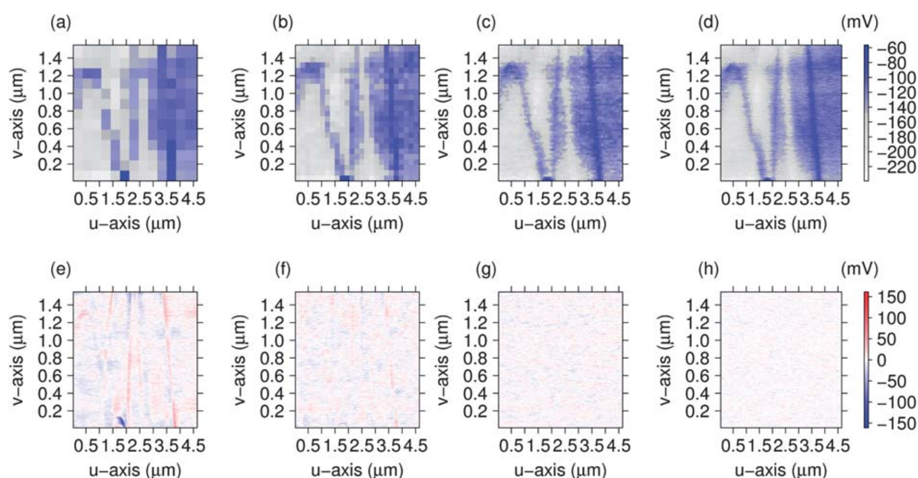

Fig. 4 Prediction of surface potential from topography information. (a–d) Surface potential maps extracted from the original data with resolutions of 13 × 13, 26 × 26, 63 × 63, and 126 × 126, respectively. (e–h) Prediction errors of high resolution (252 × 252) surface potential maps predicted from the corresponding low-resolution potential data shown in a–d.

This journal is © The Royal Society of Chemistry 2013

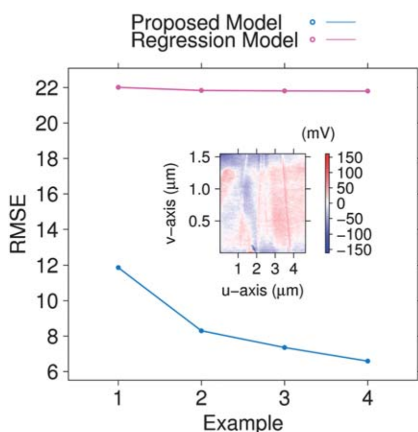

Fig. 5 Comparison of the RMSE of the proposed method to the traditional regression method for examples shown in Fig. 4. Inset: the prediction error of the regression model of the example shown in Fig. 4d.

−100 mV to 100 mV. Also, the boundaries between the NWs and the substrate are not fully eliminated from the heat images (see the red and blue regions with potential values around 100 mV and −100 mV). We note that as the image resolution increases in Fig. 4f–h, the evidence of the boundaries in Fig. 4e diminishes. Meanwhile, the predictive error decreases dramatically. By fitting the model with the highest resolution data (see Fig. 4d), we observe in Fig. 4h that the differences between the measured potential and predicted potential are close to 0 mV in the whole sample surface. To cast a direct comparison, in Fig. 5, we compute the predictive error by using the traditional regression method to fit the training data with highest resolution in Fig. 4d. As the shown in Fig. 5, there is a significant contrast between regions denoting NWs and substrate, indicating that this regression method fails to fully remove the topography pattern from the potential surface.

In addition to the graphical illustration, we compute the Root Mean Squared Error (RMSE) and summarize the results in Fig. 5. As shown in Fig. 5, the RMSE of the proposed method is universally smaller than the RMSE of the traditional regression method. From examples 1–4, the RMSE of the traditional regression method only slightly decreases from 22.01 to 21.79, compared to a 45% decrease of the RMSE of the proposed method. Based on the overwhelming performance of the proposed method, in further experiments, the predicted surface can be used to improve the spatial resolution of SPM characterizations to the level that exceeds the limit of the tool.

Conclusion

In summary, we have developed a statistical spatial model to refine and predict the nanoscale potential distribution characterized by SKPM on the surface of random lateral NW assemblies. This model addresses two important issues in nanoscale surface measurements. First, the spatial model serves to eliminate topography artifacts from SKPM raw data and retrieve the actual potential distribution. Second, based on topography measurements on dense grids, the proposed method is able to accurately predict the potential distribution with significantly enhanced spatial resolution. Statistics-enabled predictive models for nanoscale surface property characterization open new routes toward precise SPM characterizations that exceed the instrument's limitation.

Acknowledgements

The authors thank the financial support from National Science Foundation CMMI grants no. 1233570 and 1233571.

References

1 A. Noy, D. V. Vezenov and C. M. Lieber, Chemical force microscopy, *Annu. Rev. Mater. Sci.*, 1997, **27**, 381–421.
2 A. A. Gewirth and B. K. Niece, Electrochemical applications of *in situ* scanning probe microscopy., *Chem. Rev.*, 1997, **94**, 1129–1162.
3 R. C. Dunn, Near-field scanning optical microscopy, *Chem. Rev.*, 1999, **99**, 2891–2928.
4 Z. L. Wang and J. H. Song, Piezoelectric nanogenerators based on zinc oxide nanowire arrays, *Science*, 2006, **312**, 242–246.
5 K. C. Neuman and A. Nagy, Single-molecule force spectroscopy: optical tweezers, magnetic tweezers and atomic force microscopy, *Nat. Methods*, 2008, **5**, 491–505.
6 A. Majumdar, Scanning thermal microscopy, *Annu. Rev. Mater. Sci.*, 1999, **29**, 505–585.
7 G. Wittstock, M. Burchardt, S. E. Pust, Y. Shen and C. Zhao, Scanning thermal microscopy, *Angew. Chem., Int. Ed.*, 2007, **46**, 1584–1617.
8 N. Balkea, D. Bonnella, D. S. Gingera and M. Kemerink, Scanning probes for new energy materials: probing local structure and function, *MRS Bull.*, 2012, **37**, 633–637.
9 D. C. Coffey and D. S. Ginger, Time-resolved electrostatic force microscopy of polymer solar cells, *Nat. Mater.*, 2006, **5**, 735–740.
10 S. V. Kalinin and D. A. Bonnell, Imaging mechanism of piezoresponse force microscopy of ferroelectric surfaces, *Phys. Rev. B: Condens. Matter Mater. Phys.*, 2002, **65**, 125408.
11 U. Zerweck, C. Loppacher, T. Otto, S. GrafstrÃűm and L. M. Eng, Accuracy and resolution limits of Kelvin probe force microscopy, *Phys. Rev. B: Condens. Matter Mater. Phys.*, 2005, **71**, 125424.
12 E. Strassburg, A. Boag and Y. Rosenwaks, Reconstruction of electrostatic force microscopy images, *Rev. Sci. Instrum.*, 2005, **76**, 083705.
13 E. Strassburg, A. Boag and Y. Rosenwaks, Dynamics of a vibrating tip near or in intermittent contact with a surface, *Phys. Rev. B: Condens. Matter Mater. Phys.*, 2000, **61**, R13381.
14 D. J. Bayerl and X. Wang, Three-dimensional Kelvin probe microscopy for characterizing in-plane piezoelectric potential of laterally deflected ZnO micro-/nanowires, *Adv. Funct. Mater.*, 2012, **22**, 652–660.
15 S. Sadewasser, C. Leendertz, F. Streicher and M. C. Lux-Steiner, The influence of surface topography on Kelvin probe force microscopy, *Nanotechnology*, 2009, **20**, 505503.
16 B. D. Huey, C. Ramanujan, M. Bobji, J. Blendell, G. White, R. Szoszkiewicz and A. Kulik, The importance of

This journal is © The Royal Society of Chemistry 2013

distributed loading and cantilever angle in piezo-force microscopy, *J. Electroceram.*, 2004, **13**, 287–291.

17 H. O. Jacobs, P. Leuchtmann, O. J. Homan and A. Stemmer, Resolution and contrast in Kelvin probe force microscopy, *J. Appl. Phys.*, 1998, **84**, 1168–1173.

18 D. S. H. Charrier, M. Kemerink, B. E. Smalbrugge, T. de Vries and R. A. J. Janssen, Real *versus* measured surface potentials in scanning Kelvin probe microscopy, *ACS Nano*, 2008, **2**, 622–626.

19 T. Dasgupta, C. Ma, V. R. Joseph, Z. L. Wang and C. F. J. Wu, Statistical modeling and analysis for robust synthesis of nanostructures, *J. Am. Stat. Assoc.*, 2007, **103**, 594–603.

20 X. Deng, V. R. Joseph, W. Mai, Z. L. Wang and C. F. J. Wu, Statistical approach to quantifying the elastic deformation of nanomaterials, *Proc. Natl. Acad. Sci. U. S. A.*, 2009, **106**, 11845–11850.

21 S. Xu, N. Adiga, S. Ba, T. Dasgupta, C. F. J. Wu and Z. L. Wang, Optimizing and improving the growth quality of ZnO nanowire arrays guided by statistical design of experiments, *ACS Nano*, 2009, **3**, 1803–1812.

22 F. Wang, Y. Hwang, P. Z. G. Qian and X. Wang, A statistics-guided approach to precise characterization of nanowire morphology, *ACS Nano*, 2010, **4**, 855–C862.

23 W. Mai and X. Deng, Applications of statistical quantification techniques in nanomechanics and nanoelectronics, *Nanotechnology*, 2010, **21**, 1246–1266.

24 J. Song, H. Xie, W. Wu, V. R. Joseph, C. F. J. Wu and Z. L. Wang, Robust Optimization of the output voltage of nanogenerators by statistical design of experiments, *Nano Res.*, 2010, **3**, 613–619.

25 T. Dasgupta, B. Weintraub and V. R. Joseph, A physical statistical model for density control of nanowires, *IIE Transactions*, 2011, **43**, 233–241.

26 Q. Huang, L. Wang, T. Dasgupta, L. Zhu, P. K. Sekhar, S. Bhansali and Y. An, Statistical weight kinetics modeling and estimation for silica nanowire growth catalyzed by Pd thin film, *IEEE Transactions in Automation Science and Engineering*, 2011, **8**, 303–310.

27 X. Xu, Y. Hwang, T. Kim, F. Wang, X. Wang P. Z. G. Qian. Sequential synthesis of nanomaterials *via* level-expansion. 2011 submitted manuscript.

28 C. J. Chang, L. Xu, Q. Huang and J. Shi, Quantitative characterization and modeling strategy Of nanoparticle dispersion in polymer composites, *IIE Transactions*, 2012, **44**, 523–535.

29 G. Koley, M. G. Spencer and H. R. Bhangale, Cantilever effects on the measurement of electrostatic potentials by scanning Kelvin probe microscopy, *Appl. Phys. Lett.*, 2001, **7**, 545–547.

30 G. Matheron, Principles of geostatistics, *Econ. Geol.*, 1963, **58**, 1246–1266.

31 J. Sacks, W. Welch, T. J. Mitchell and H. P. Wynn, Design and analysis of computer experiments, *Stat. Sci.*, 1989, **4**, 409–423.

32 W. J. Welch, R. J. Buch, J. Sacks, H. P. Wynn, T. J. Mitchell and M. D. Morris, Screening, predicting and computer experiments, *Technometrics*, 1992, **34**, 15–25.

33 T. J. Santner, B. J. Williams and W. Notz, *Design and Analysis of Computer Experiments*, Springer-Verlag, Berlin Heidelberg, 1st edn, 2003.

34 J. P. C. Kleijnen, *Design and Analysis of Simulation Experiments*, Springer Publishing Company, Incorporated, 1st edn, 2007.

35 M. Stein, *Interpolation of Spatial Data, Some Theory for Kriging. Springer Series in Statistics*, Springer, New York, 1999.

 This journal is © The Royal Society of Chemistry 2013